Journal of Marine Science and Technology

Volume 25 | Issue 4 Article 6

NON-PARAMETRIC IDENTIFICATION OF NONLINEAR DAMPING AND RESTORING FORCES FOR SHIP FREE ROLL DECAY IN NUMERICAL TANK

Yin Jiang
Innovation Center for Advanced Ship and Deep-Sea Exploration. The State Key Laboratory of Ocean Engineering, Shang Hai Jiao Tong University.

Ren-Chuan Zhu
Innovation Center for Advanced Ship and Deep-Sea Exploration. The State Key Laboratory of Ocean Engineering, Shang Hai Jiao Tong University.

Guo-Ping Miao
Innovation Center for Advanced Ship and Deep-Sea Exploration. The State Key Laboratory of Ocean Engineering, Shang Hai Jiao Tong University.

Ju Fan
Innovation Center for Advanced Ship and Deep-Sea Exploration. The State Key Laboratory of Ocean Engineering, Shang Hai Jiao Tong University.

Chao Ma
Innovation Center for Advanced Ship and Deep-Sea Exploration. The State Key Laboratory of Ocean Engineering, Shang Hai Jiao Tong University.

Recommended Citation

Jiang, Yin; Zhu, Ren-Chuan; Miao, Guo-Ping; Fan, Ju; and Ma, Chao (2017) "NON-PARAMETRIC IDENTIFICATION OF NONLINEAR DAMPING AND RESTORING FORCES FOR SHIP FREE ROLL DECAY IN NUMERICAL TANK," *Journal of Marine Science and Technology*: Vol. 25: Iss. 4, Article 6.
DOI: 10.6119/JMST-017-0317-2
Available at: https://jmstt.ntou.edu.tw/journal/vol25/iss4/6

NON-PARAMETRIC IDENTIFICATION OF NONLINEAR DAMPING AND RESTORING FORCES FOR SHIP FREE ROLL DECAY IN NUMERICAL TANK

Acknowledgements

This work has been supported by National Natural Science Foundation of China (NSFC, Grant no. 51479117, 51579147) and National Key Basic Research Program of China (973 Program, Grant no. 2014CB046203)

Journal of Marine Science and Technology, Vol. 25, No. 4, pp. 404-416 (2017)
DOI: 10.6119/JMST-017-0317-2

NON-PARAMETRIC IDENTIFICATION OF NONLINEAR DAMPING AND RESTORING FORCES FOR SHIP FREE ROLL DECAY IN NUMERICAL TANK

Yin Jiang[1, 2], Ren-Chuan Zhu[1, 2], Guo-Ping Miao[1, 2], Ju Fan[1, 2], and Chao Ma[1, 2]

Key words: free roll decay, overset mesh technology, nonlinear roll damping and restoring.

ABSTRACT

Numerical simulations of free roll decay are carried out for the DTMB 5512 based on computational fluid dynamics (CFD) theory and adoption of overset mesh technology. The numerical time history of the ship roll shows good quantitative agreement with the experimental time history in the case of Fr = 0.138 with an angle of list of $\theta_{a0} = 10°$. The natural period is well estimated, there is less than 2% error. According to the time history of the roll angle and the corresponding angular velocity, the nonlinear ship roll damping and restoring force of the hull are identified by solving the nonlinear Volterra integral equation of the first kind with Tikhonov's regularization method. The results indicate that the numerical method in the paper is feasible, and the choice of regularization parameter is proper. Additionally, the influences of angle of list, model scale and ship speed on free roll decay are investigated. Roll damping and nonlinear restoring force increase as model scale decreases. Keeping the same scale of ship model, roll damping increases with ship speed while nonlinear restoring force decreases.

I. INTRODUCTION

It is necessary to obtain an accurate roll damping before making a good evaluation of roll motion. Traditionally, there are three kinds of methods available for estimating the roll damping, the model test (Irvine, 2004; Aloisio and Felice, 2006; Irvine et al., 2013; de Oliveira and Fernandes, 2014), the semi-empirical method (Ikeda et al., 1976; Ikeda et al., 1977; Ikeda et al., 1977; Ikeda et al., 1978), and the numerical method (Yang et al., 2012; Zhu et al., 2012; Yang et al., 2013). The model test is a quite reliable method, but costs both time and money. The semi-empirical method is a convenient way to evaluate the ship roll damping by summing up each individual component, but it neglects the interactions among each component, and the roll damping cannot be evaluated accurately, especially when the roll angle is large. However, with the development of computational science and technology, the numerical simulation method, which is based on the computational fluid dynamic, is developing rapidly. More and more dynamic mesh technologies, especially overset mesh technology, have been implemented in the simulation of an object in motion. In recent years, overset mesh technology has been applied in numerical simulations of a ship in roll motion. Chen et al. (2001) carried out numerical simulations of two types of roll motion, a barge- prescribed roll and free roll decay. Wilson et al. (2006) performed simulations of free roll decay and forced roll of the DTMB 5512 with/without bilge keel to show that the numerical method that is used on paper can accurately estimate the natural rolling frequency and roll decay rate at various ship speeds. Jiang et al. (2016) conducted simulations of free roll decay of DTMB 5512 with bilge keel to explore the characteristics of roll damping. Meanwhile, verification and validation (V & V) of numerical results are required, the procedure for the CFD uncertainty analysis, which is provided by Stern et al. (1999; 2001), is considered to be widely accepted and available.

Generally, the time history of free roll decay can be obtained from a free roll decay test, either a model test or a numerical test. Roll damping can be evaluated with either the extinction curve method (Zhu et al., 2012; Yang et al., 2013; Jiang, 2016) or the energy method (Ma et al., 2012; Jiang et al., 2016) , in which the two following roll damping models are usually adopted (Zhou, 2012). One is the linear-plus-quadratic damping model, $M(\theta') = b_1\theta' + b_2|\theta'|\theta'$, and the other is the linear-plus-cubic damping model, $M(\theta') = b_1\theta' + b_3\theta'^3$. Roll damping estimations based on the damping model can be regarded as parametric identification (Li et al., 2012; Hou, 2015; 2016; Jiang and Zhu et al., 2016). Li et al. (2012) focused on the estimation method of least square support vector regression (LS-SVR) theory to identify the parameters of roll motion based on the linear-plus-quadratic roll

Paper submitted 11/02/16; revised 02/24/17; accepted 03/17/17. Author for correspondence: Ren-Chuan Zhu (E-mail: renchuan@sjtu.edu.cn).
[1] Innovation Center for Advanced Ship and Deep-Sea Exploration.
[2] The State Key Laboratory of Ocean Engineering, Shang Hai Jiao Tong University.

damping model. Hou et al. (2015) also aimed at identification method- support vector regression (SVR) to identify the nonlinear roll motion equation with linear-plus-quadratic roll damping model for a FPSO vessel in regular waves. Jang (2011) pointed out that parametric identification is limited to finding only the parameters on which the systems are assumed to depend, that is, the model should be given in advance. Taylan (1998) investigated various representations of the damping and restoring terms, results showed that an inappropriate selection of damping and restoring terms may lead to a serious discrepancy with reality, especially in peak roll amplitudes. Unlike parametric identification, non-parametric identification is a good method. It requires no priori assumption about the form of damping, with only the displacement and velocity being required. Jang (2011) also proposed a method to identify nonlinear damping by solving the nonlinear Volterra integral equation of the first kind, and applied this method only in the identification of roll damping of a fishing vessel in free roll decay (Jang et al., 2010). As for the nonlinear Volterra integral equation of the first kind, that inverse problem is ill-posed, the solutions lack numerical stability (Tikhonov, 1963; Groetsch, 1993). In order to suppress the instability of the inverse problem, many regularization methods (e.g., Tikhonov' regularization method, Landweber's regularization method etc.) are developed and applied (Groetsch, 1993). Jang (2009; 2013) used Landweber's regularization method to overcome the instability problem encountered when solving a nonlinear Volterra integral equation of the first kind.

In the present paper, a new analytical approach for the free roll decay of ships is established, in which roll histories are obtained by numerical simulations of the free roll decay of ships by adopting the overset mesh technology. Then nonlinear Volterra integral equation of the first kind with Tikhonov's regularization method is solved to identify the nonlinear roll damping and restoring forces. The approach is extended to be applied in evaluating the influence of parameters (e.g., angle of list, scale and speed etc.) on the ship rolling. More specifically, the numerical simulation of free roll decay of the DTMB 5512 with bilge keel at Fr = 0.138 is firstly performed, given an angle of list of θ_{a0} = 10° . That case is selected for V & V to verify the validity of the numerical method used in the paper. Secondly, given the angle of list of θ_{a0} = 2.5°, 5°, 7.5°, 12.5°, 15°, and 20°, numerical simulations of the free roll decay of the ship without forward speed are performed. Both the nonlinear damping and restoring force of the hull in free roll decay are identified by solving a nonlinear Volterra integral equation of the first kind with Tikhonov's regularization method with a proper regularization parameter, $\chi^2 = 0.01$. Furthermore, the effects of scale and speed on the roll damping and nonlinear restoring force are discussed, respectively.

II. GOVERNING EQUATION AND REALIZATION OF ROLL MOTION OF THE SHIP

The finite volume method is used in deriving discretized equations. The second-order upwind scheme is adopted in the convection term, and the central-differencing scheme is used in the diffusion term. The coupled equation of velocity and pressure is solved by the Semi-Implicit Method for Pressure-Linked Equations (SIMPLE algorithm). The volume of fluid method (VOF) is used to distinguish between two different phases. The algebraic multigrid method is used to solve the discretized algebraic equations.

1. Governing Equation

Continuity equation:

$$\frac{\partial \rho}{\partial t}+\frac{\partial(\rho \overline{u}_i)}{\partial x_i}=0 \quad (i=1, 2, 3) \tag{1}$$

Momentum equation:

$$\frac{\partial(\rho \overline{u}_i)}{\partial t}+\frac{\partial(\rho \overline{u}_i \overline{u}_j)}{\partial x_j}=\frac{\partial}{\partial x_j}\left[\mu \frac{\partial \overline{u}_i}{\partial x_j}-\rho \overline{u_i' u_j'}\right] -\frac{\partial \overline{p}}{\partial x_i}+\rho f_i \quad (i, j=1, 2, 3) \tag{2}$$

Transport equation of a scalar quantity $\overline{\Phi}$:

$$\frac{\partial(\rho \overline{\Phi})}{\partial t}+\frac{\partial(\rho \overline{u}_j \overline{\Phi})}{\partial x_j}=\frac{\partial}{\partial x_j}\left(\mu \frac{\partial \overline{\Phi}}{\partial x_j}-\rho \overline{u_j' \Phi'}\right)+S \tag{3}$$

in which $\overline{u}_i$ is velocity in i th direction, f_i stands for the body force, $\overline{p}$ is the pressure, density is defined as $\rho=\sum_{q=1}^{2} a_q \rho_q$, in which the volume fraction a_q represents the volume proportion of the q-th phase fluid in a cell, and $\sum_{q=1}^{2} a_q=1$, and μ is the average dynamic viscosity with its form being analogous to that of the density.

Returning to Eq. (3) and introducing the turbulent kinetic energy k and the dissipation rate ω respectively, the SST k-ω model is derived as follows:

$$\frac{\partial}{\partial t}(\rho k)+\frac{\partial}{\partial x_i}(\rho k \overline{u}_i)=\frac{\partial}{\partial x_j}\left(\Gamma_k \frac{\partial k}{\partial x_j}\right)+G_k-Y_k$$

$$\frac{\partial}{\partial t}(\rho \omega)+\frac{\partial}{\partial x_i}(\rho \omega \overline{u}_i)=\frac{\partial}{\partial x_j}\left(\Gamma_\omega \frac{\partial \omega}{\partial x_j}\right)+G_\omega-Y_\omega+S_\omega \tag{4}$$

$(i=1, 2, 3)$

where the diffusivity of k, diffusivity of ω, production of k, production of ω, dissipation of k, dissipation of ω, and cross

Table 1. Principal particulars of DTMB 5512.

Main Features	Value	Main Features	Value
Scale λ	46.588	Draft T (m)	0.132
Length between perpendiculars L (m)	3.048	Wetted surface S (m^2)	1.371
Vertical position of gravity center z_g (m)	0.030	Block coefficient C_b	0.506
Beam B (m)	0.405	Mass m (kg)	82.150

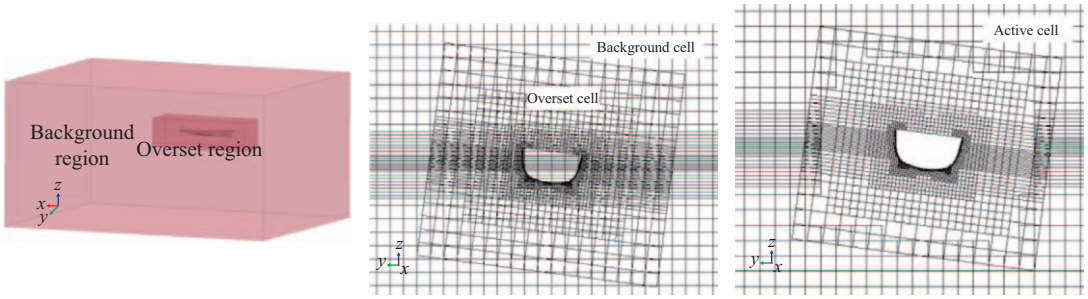

Fig. 1. overset mesh schematic.

diffusion term , are denoted by Γ_k, Γ_ω, G_k, G_ω, Y_k, Y_ω, and S_ω, respectively.

The transport equation of the volume of fraction can be written as

$$\frac{\partial a_q}{\partial t}+\frac{\partial(\overline{u}_i a_q)}{\partial x_i}=0 \quad (q=1,2;\ i=1,2,3) \tag{5}$$

2. Roll Decay Motion Equation

In the system of the ship in free roll decay, assuming the hull is treated as a rigid body, a reference coordinate system, denoted by *OXYZ*, is fixed at the gravity center of the hull. It follows the right-hand rule, the positive *X* direction is towards the stern and the positive *Y* direction is towards the starboard. By application of the Newton's second Law, the roll decay motion equation is defined as

$$I_{xx}\frac{d\theta'}{dt}=\iint_s f(r_2n_3-r_3n_2)dS \tag{6}$$

where I_{xx} stands for the moment of inertia around the *X*-axis, θ' represents the roll angular velocity, f is the stress acted on the wetted surface of the hull, which is composed of dynamic pressure and shear stress. The normal of the element on the hull is marked as $\vec{n}=(n_1,n_2,n_3)$, and $\vec{r}=(r_1,r_2,r_3)$ denotes the coordinates of the center of the element on the hull in the reference frame.

3. Overset Methodology

Overset meshes are used to discretize a computational domain with several different meshes that overlap each other in an arbitrary manner (CD-adapco, 2014). There are two kinds of regions in the overset meshes, a background region enclosing the entire solution domain and one or more overset regions containing the bodies within the domain, as shown in Fig. 1(a). The cell generated in the background region is called the background cell, whereas the cell in the overset region is referred to as the overset cell.

In a set of overset mesh, cells are grouped into active and inactive cells. Discretized governing equations are solved within active cells, as shown in Fig. 1(c). The difference between Figs. 1(b) and (c) is that the background cells within the overset region where two different sets of cells overlap are cleared up. The cells within which no equation is solved are known as inactive cells. Acceptor cells separate active and inactive cells in the background region and are attached to the overset boundary in the overset region (CD-adapco, 2014). Acceptor cells contribute to the information exchange between the background region and the overset region. Variable values at the acceptor cell of one mesh are expressed by variable values at donor cells in the other mesh through linear interpolation, yielding

$$\varphi_{rec}=\sum\xi_i\varphi_i \tag{7}$$

where φ_{rec} is the variable values at the acceptor cells, φ_i is the variable values at the donor cells, and ξ_i is the shape functions spanning a triangle (in 2D) or a tetrahedron (in 3D) defined by the centroids of the donor cells.

III. GEOMETRY AND MESH

1. Geometry and Case Conditions

The US Navy combatant, DTMB 5512, is only equipped with bilge keel B whose details can be found in the reference (2008). Principle particulars for the DTMB 5512 are listed in Table 1. Numerical simulation conditions for free roll decay motion tests are summarized in Table 2.

Table 2. Conditions for numerical simulation of roll decay motion.

	Scale	Fr	Angle of list (deg)
Free roll decay	46.588	0/0.138/0.28	2.5/5.0/7.5/10.0/12.5/15.0/20.0
	35.482/24.830/13.311	0	2.5/5.0/7.5/10.0/12.5/15.0/20.0

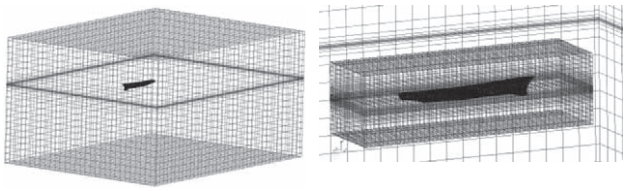

Fig. 2. Mesh generation.

2. Mesh and Domain

In the cases of free roll decay, the whole flow field was discretized. The space coordinate range for background region is determined as $-2\frac{1}{2}L < X < 1\frac{1}{2}L$, $-L < Y < L$, $-L < Z < \frac{2}{3}L$, and the overset region of 5512 is determined as $-\frac{3}{4}L < X < \frac{3}{4}L$, $-\frac{2}{3}B < Y < \frac{2}{3}B$, $\frac{1}{5}L < Z < \frac{1}{5}L$. Fig. 2 depicts overset meshes of the objective hulls. In the regions, i.e., free surface zones or regions near the hull, some variable gradients are large. The cells in these regions need to be refined, in order to either capture the free surface precisely or compute the force acted on the hull accurately. Moreover, the cells in the overlapping region are of similar size in both the background and overset meshes.

3. Boundary Condition

The computational domain is discretized, boundary conditions are set up as follows:

(1) Inlet/lateral/bottom/top boundaries:
The velocity vector is specified directly, pressure is extrapolated from the adjacent cell using reconstruction gradients.
(2) Outlet boundary:
The velocity is extrapolated from the interior using reconstruction gradients. Pressure is specified.
(3) Ship hull boundary:
The tangential velocity is explicitly set to zero. Pressure is extrapolated from the adjacent cell using reconstruction gradients.

IV. IDENTIFY NON-LINEAR DAMPING AND RESTORING FORCE

1. Modeling of Nonlinear Damping and Restoring Force

Supposing the system of the hull in free roll decay is nonlinear, the application of Newton's second law yields the following second-order ordinary differential equation with the following initial conditions.

$$I_{xx}\theta'' + C\theta = M(\theta') + r(\theta) \tag{8}$$

and

$$\theta(0) = \alpha \qquad \theta'(0) = \beta \tag{9}$$

where C represents the restore coefficient and θ, θ', θ'' are corresponding to the roll angle, the roll angular velocity, and the roll angular acceleration, respectively. $M(\theta')$ denotes the roll damping moment, which is a function of the roll angular velocity. $r(\theta)$ represents the nonlinear restoring force. Both the nonlinear damping $M(\theta')$ and nonlinear restoring force $r(\theta)$ have an anti-symmetry property:

$$M(-\theta') = -M(\theta') \tag{10}$$

$$r(-\theta) = -r(\theta) \tag{11}$$

Defined here, $\Phi(t) = M(\theta') + r(\theta)$, an equivalent form of Eq. (8), is rewritten as

$$I_{xx}\theta'' + C\theta = \Phi(t) \tag{12}$$

According to the concept of variation of constants, the solution of the inhomogeneous Eq. (12) is supposed to be

$$\theta = \upsilon_1\theta_1 + \upsilon_2\theta_2, \qquad \theta' = \upsilon_1\theta_1' + \upsilon_2\theta_2' \tag{13}$$

where θ_1 and θ_2 satisfy the homogeneous equation $I_{xx}\theta'' + C\theta = 0$ and υ_1 and υ_2 are unknown functions of t. The first equation in Eq. (13) is differentiated as

$$\theta' = \upsilon_1'\theta_1 + \upsilon_1\theta_1' + \upsilon_2'\theta_2 + \upsilon_2\theta_2' \tag{14}$$

Comparing Eq. (14) and the second equation in Eq. (13), the first condition on υ_1 and υ_2 is as follows:

$$\upsilon_1'\theta_1 + \upsilon_2'\theta_2 = 0 \tag{15}$$

Substituting Eq. (13) into (12) yields the second condition on υ_1 and υ_2:

$$\upsilon_1'\theta_1' + \upsilon_2'\theta_2' = \frac{\Phi}{I_{xx}} \tag{16}$$

The solutions to Eq. (15) and Eq. (16) are obtained by

$$\begin{bmatrix} \upsilon_1' \\ \upsilon_2' \end{bmatrix} = \begin{bmatrix} \theta_1 & \theta_2 \\ \theta_1' & \theta_2' \end{bmatrix}^{-1} \begin{bmatrix} 0 \\ \dfrac{\Phi}{I_{xx}} \end{bmatrix} = \frac{M(\theta') + r(\theta)}{I_{xx}W} \begin{bmatrix} -\theta_2 \\ \theta_1 \end{bmatrix} \tag{17}$$

in which the Wronskian $W = \theta_1\theta_2' - \theta_2\theta_1'$, a nonlinear Volterra integral equation, is derived by integrating Eq. (17) and substituting it into the first equation in Eq. (13):

$$\theta(t) = \alpha\theta_1(t) + \beta\theta_2(t) + \int_0^t \frac{\theta_1(\tau)\theta_2(t) - \theta_1(t)\theta_2(\tau)}{I_{xx}W}\left[M(\theta') + r(\theta)\right]d\tau \tag{18}$$

where θ_1 and θ_2 are chosen to ensure that

$$\begin{aligned} I_{xx}\theta_1'' + C\theta_1 &= 0, \qquad \theta_1(0) = 1,\ \theta_1'(0) = 0 \\ I_{xx}\theta_2'' + C\theta_2 &= 0, \qquad \theta_2(0) = 1,\ \theta_2'(0) = 0 \end{aligned} \tag{19}$$

so that the form of θ_1 and θ_2 are as follows:

$$\begin{aligned} \theta_1 &= \cos(\omega t) \\ \theta_2 &= \frac{1}{\omega} * \sin(\omega t) \end{aligned} \tag{20}$$

in which $\omega = \sqrt{C / I_{xx}}$.

2. Identify Nonlinear Damping and Restoring Force

The kernel, $K(t, \tau)$, is defined as

$$K(t, \tau) = \frac{\theta_1(\tau)\theta_2(t) - \theta_1(t)\theta_2(\tau)}{I_{xx}W} \tag{21}$$

Then Eq. (18) is rewritten as

$$\theta(t) - \alpha\theta_1(t) - \beta\theta_2(t) = \int_0^t K(t, \tau)\Phi(\tau)d\tau \tag{22}$$

which is classified as the Volterra integral equation of the first kind for Φ.

Two unknowns are involved in this nonlinear equation, the nonlinear damping $M(\theta')$ and the restoring force $r(\theta)$. An ingenious approach (Jang, 2011) is used to solve two unknowns, respectively.

Given histories of the roll angle and roll angular velocity, a number of intersection points of the roll angle/roll angular velocity curve with the x-axis are obtained. The t_l for $l = 1, 2, \ldots$ is a zero-crossing time for the roll angle, and t_m for $m = 1, 2, \ldots$ is a zero-crossing time for the roll angular velocity.

$$\theta(t_l) = 0 \quad for \quad l = 1, 2, \ldots \tag{23}$$

$$\theta'(t_m) = 0 \quad for \quad m = 1, 2, \ldots \tag{24}$$

Considering the anti-symmetry property, when the roll angle is zero,

$$\begin{aligned} &r(-\theta(t_l) = 0) - r(\theta(t_l) = 0) = 0 \\ &\Phi(t_l) = M(\theta'(t_l)) \end{aligned} \tag{25}$$

Similarly, when the roll angular velocity is zero,

$$\begin{aligned} &M(-\theta'(t_m) = 0) - M(\theta'(t_m) = 0) \\ &\Phi(t_m) = r(\theta(t_m)) \end{aligned} \tag{26}$$

3. Tikhonov's Regularization

The nonlinear integral Eq. (22) should be discretized, given the signal at $t = t_1, t_2, \ldots t_n$, the trapezoidal rule is adopted to approximate the integral term. Then the matrix equation is derived as

$$\eta = L\Phi \tag{27}$$

where η is the vector which is the left hand side in Eq. (22) evaluated at $t = t_1, t_2, \ldots t_n$.

$$L_{ij} = q_j K(t_i, t_j)\Delta t \tag{28}$$

$$q_j = \begin{cases} 0.5 & j = 1, i \\ 1 & 1 < j < i \\ 0 & otherwise \end{cases} \tag{29}$$

That is an ill-posed problem, and the solution of Eq. (27) is not unique. In solving such inverse problems, a regularization term can be included in the minimization process in order to give preference to a particular solution with desirable properties.

$$\min\left(\left\|L\Phi - \eta\right\|^2 + \left\|\Gamma\Phi\right\|^2\right) \tag{30}$$

Table 3. Number of grids in simulation (10^4).

	Coarse	medium	fine
Background region	6.8	16.7	42.8
Overset region	34.5	64.6	138.1

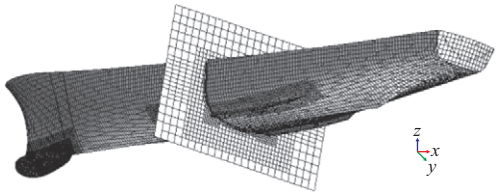

(a) coarse grids

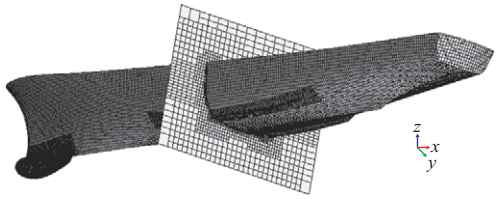

(b) middle grids

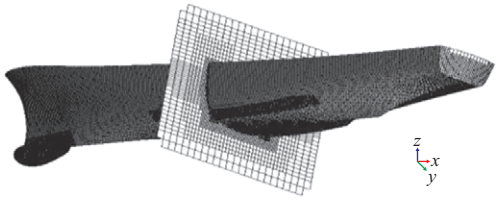

(c) fine grids

Fig. 3. Grids on hull and middle section.

where Γ is the Tikhonov matrix, which is chosen as a multiple of the identity matrix $\Gamma = \chi I$, $\|L\Phi - \eta\|^2$ represents the error from the mathematical model, $\|\Gamma\Phi\|^2$ is a L2 norm which reflects the smoothness of the solution, and χ is chosen to balance the two effects.

Defined here, $E = \|L\Phi - \eta\|^2 + \|\Gamma\Phi\|^2$, then

$$\begin{aligned} E &= (\eta - L\Phi)^T(\eta - L\Phi) + (\Gamma\Phi)^T(\Gamma\Phi) \\ &= \eta^T\eta - 2\eta^T L\Phi + \Phi^T L^T L\Phi + \Phi^T\Gamma^T\Gamma\Phi \end{aligned} \tag{31}$$

In order to obtain the extremum, the derivative of Eq. (31) needs to be zero:

$$\begin{aligned} &\nabla E = 0 \\ &-2(\eta^T L)^T + L^T\Gamma\Phi + (L^T L)^T\Phi + 2\Gamma^T\Gamma\Phi = 0 \\ &(L^T L + \Gamma^T\Gamma)\Phi = L^T \\ &\Phi = (L^T L + \Gamma^T\Gamma)^{-1} L^T\eta \end{aligned} \tag{32}$$

If both the angular acceleration and the roll angle are given, Φ_ref is a reference vector whose components can be calculated out directly according to the left hand side of Eq. (8). $\Phi(t)$ is obtained from Eq. (32), then the optimal value of the regularization parameter is chosen according to Eq.(33).

$$\arg_{\chi^2} \min \|\Phi - \Phi\_ref\|_2^2 \tag{33}$$

V. ANALYSIS OF RESULTS

1. Uncertainty Analysis of Numerical Results

For the problem of the roll decay motion of the hull with speed, the attitude is considered in the progress of geometry construction. The simulation involves two stages. In the first stage, the hull is fixed with an initial heel. For the second stage, the hull is in the roll decay motion.

The case which $\theta_0 = 10°$ and, Fr = 0.138 is selected for V & V. In order to obtain the numerical error/uncertainties of the simulations, at least three different sets of grids are required, as displayed in Fig. 3. The refinement factor of grids is $\sqrt{2}$, the numbers of grids for the case are listed in Table 3.

The solutions of fine/medium/coarse grids are expressed with $S_{G1}/S_{G2}/S_{G3}$, and three time steps $\Delta t_1 = 0.005$, $\Delta t_2 = 0.0071$, and $\Delta t_3 = 0.01$ are available. Grid errors/uncertainties (δ_G/U_G) are estimated from the results of multiple grids while keeping the fine time step, $\Delta t_1 = 0.005$, constant. The errors/uncertainties (δ_T/U_T) of the time steps are estimated by refining the time step while keeping the grid S_{G2} constant.

Verification is performed with consideration to grid and time step convergence studies. Numerical simulation errors δ_{SN} and uncertainties U_{SN} are given by

$$\begin{aligned} \delta_{SN} &= \delta_G + \delta_T \\ U_{SN}^2 &= U_G^2 + U_T^2 \end{aligned} \tag{34}$$

A global convergence ratio $\langle R_G \rangle = \|\varepsilon_{21G}\|_2 / \|\varepsilon_{31G}\|_2 = 3.734/10.899 \approx 0.343$, $< >$ denotes an averaged value and $\|\varepsilon\|_2 = \left[\sum_{i=1}^{N} \varepsilon_i^2\right]^{1/2}$ denotes the L2 norm of solution change over the N points in the first five periods of free roll decay. $\langle R_G \rangle < 1$ indicates that the convergence condition is monotonic convergence. The order of accuracy $\langle P_G \rangle$ and the correction factor $\langle C_G \rangle$ are:

$$\langle P_G \rangle = \frac{\ln\left(\|\varepsilon_{32G}\|_2 / \|\varepsilon_{21G}\|_2\right)}{\ln r_G} \approx 3.090 \tag{35}$$

$$\langle C_G \rangle = \frac{r_G^{\langle P_G \rangle} - 1}{r_G^{\langle P_{G_{est}} \rangle} - 1} \approx 1.918 \tag{36}$$

Table 4. Averaged values from verification of free roll decay for Fr = 0.138 with angle of list θ_{a0} = 10°.

Study	R_G	P_G	C_G	U_G	R_{GC}
Grid	0.34	3.09	1.92	1.66%	0.54%
TimeStep	0.51	1.94	0.96	0.60%	0.02%

Table 5. Averaged values from validation of free roll decay for Fr = 0.138 with angle of list θ_{a0} = 10°.

	E%	U_V%	U_D%	U_{SN}%
$E = D - S$	-0.676	2.458	1.5	1.771
$E_C = D - S_C$	-0.581	1.628	1.5	0.539

where $P_{Gest} = 2$ is the theory accuracy.

For $\langle C_G \rangle \approx 1.918$, when considered as sufficiently less than or greater than 1 and lacking confidence, U_G is estimated and not δ_G^*.

$$U_G = \left| \langle C_G \rangle \left(\frac{\varepsilon_{21G}}{r_G^{\langle P_G \rangle} - 1} \right) \right| + \left| \left(1 - \langle C_G \rangle\right) \left(\frac{\varepsilon_{21G}}{r_G^{\langle P_G \rangle} - 1} \right) \right| \quad (37)$$

For $\langle C_G \rangle \approx 1.918$, when considered close to 1 and having confidence, both δ_G^* and U_{GC} are estimated:

$$\delta_G^* = \langle C_G \rangle \left(\frac{\varepsilon_{21G}}{r_G^{\langle P_G \rangle} - 1} \right) \quad (38)$$

$$U_{CG} = \left| \left(1 - \langle C_G \rangle\right) \left(\frac{\varepsilon_{21G}}{r_G^{\langle P_G \rangle} - 1} \right) \right| \quad (39)$$

Verification for the results of the different time steps is performed by the same process. The results are summarized in Table 4. The results show that the errors/uncertainties due to grids are the main components by comparing the differences of the errors/uncertainties of grids and time steps.

Validation of the free roll decay is performed by using both the simulation prediction S and the corrected simulation prediction S_C. Averaged values for both definitions of the comparison error, validation uncertainty, and simulation uncertainty are given in Table 5. Values are normalized with $2\theta_{\alpha 0}$. The point comparison error $E = D - S_{G2}$ is compared to the validation uncertainty U_V in Fig. 4(a), while the error $E_C = D - S_C$ is compared to the validation uncertainty U_{VC} in Fig. 4(b), in which the uncertainty of the model test is U_D = 1.5% (Wilson et al., 2006; Zhu et al., 2015). The simulation results for both the uncorrected and corrected approaches are validated, at a level of 2.458% and 1.628%, respectively.

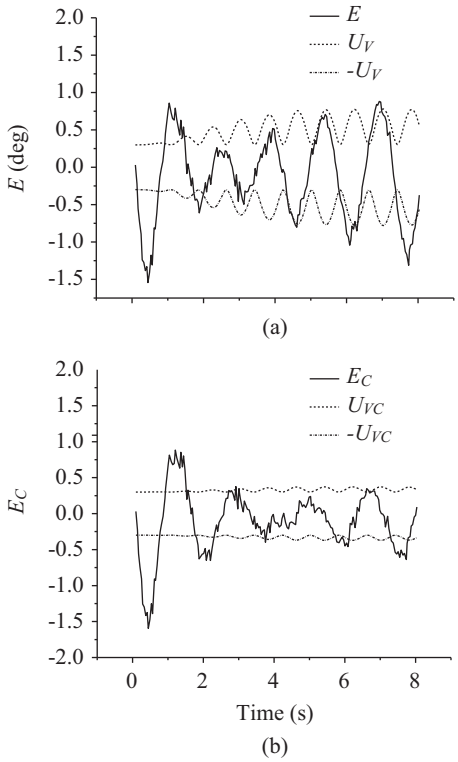

Fig. 4. Validation for free roll decay with angle of list θ_{a0} = 10° at Fr = 0.138.

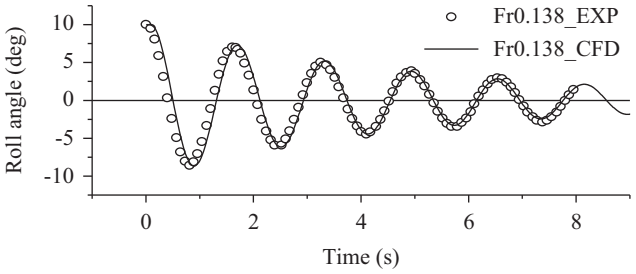

Fig. 5. Roll history (Fr = 0.138, θ_{a0} = 10°).

The numerical result S_{G2} is in good agreement with the experimental one, as shown in Fig. 5. From the roll time history, the amplitude in the previous roll cycles decays faster, while it decays slower after several cycles. The average of the first five roll cycles is defined as the natural roll period, its numerical quantity is 1.6125 s and the experimental quantity is 1.6402 s, the error between these two is less than 2%.

2. Influence of Angle of List

In order to take the consideration of the initial condition, numerical simulations of free roll decay at Fr = 0 with different angle of lists, θ_{a0} = 2.5°, 5.0°, 7.5°, 10.0°, 12.5°, 15.0°, 20.0°, are performed. The histories of the roll angle and roll angular velocity are monitored, as displayed in Fig. 6. Assuming a series of candidates, $\chi^2 = 10^{-1}, 10^{-2}, 10^{-3}, 10^{-4}, 10^{-5}, 10^{-6}$, $\left\| \Phi - \Phi\_ref \right\|_2^2$ with various χ^2 is tabulated in Table 6. Based on Eq. (33), the

Table 6. influence of χ^2 on value of $\|\Phi - \Phi\_ref\|_2^2$ for different angle of list.

χ^2 / Angle of list	10^{-1}	10^{-2}	10^{-3}	10^{-4}	10^{-5}	10^{-6}
2.5	2	2	4	12	33	86
5	10	7	15	46	132	348
7.5	27	18	33	105	299	797
10	49	31	58	186	542	1438
12.5	104	59	93	289	825	2172
15	155	88	143	429	1233	3284
20	306	158	261	761	2119	5602

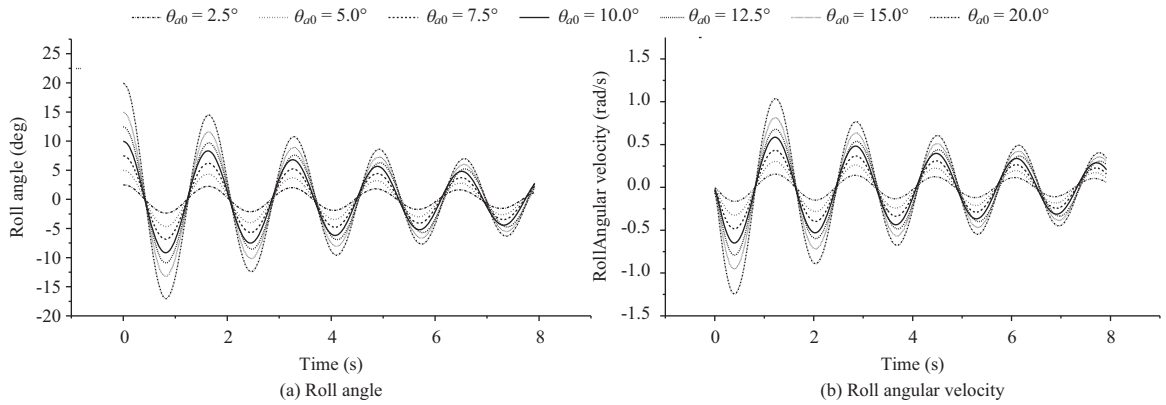

Fig. 6. Time history.

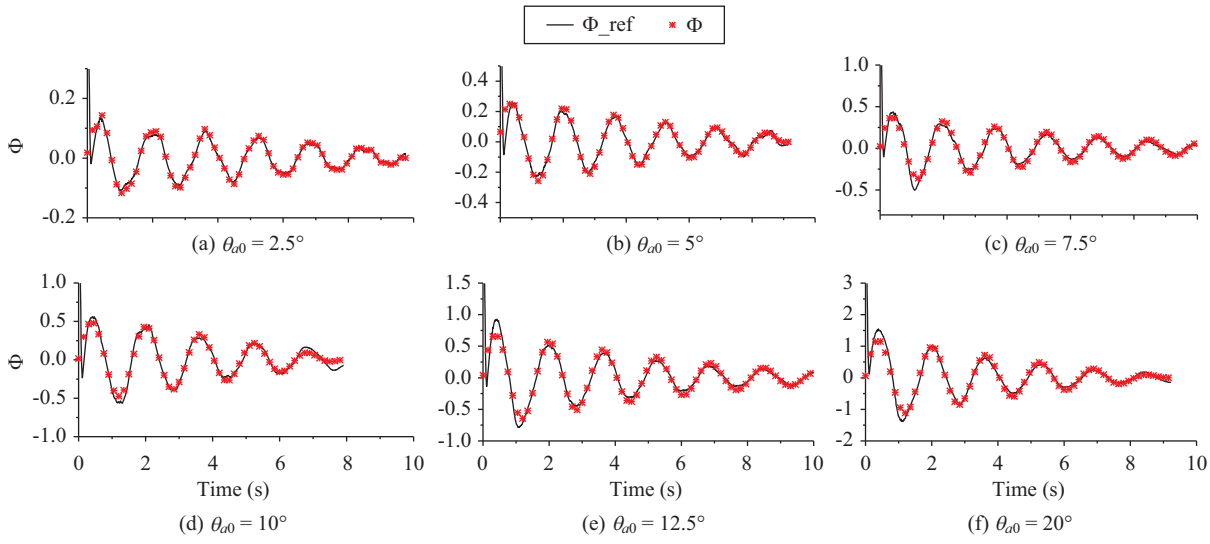

Fig. 7. Solutions of Φ for different angle of list (χ^2 = 0.01).

optimal regularization parameter is set as 0.01. Φ agrees well with Φ_*ref*, as shown in Fig. 7.

According to Eqs. (25) and (26), the nonlinear damping $M(\theta')$ and the restoring force $r(\theta)$ are derived, as shown in Figs. 8 and 9. Based on the non-parametric model, each set of data is fitted with a polynomial form to a curve, and a fitting formula is indicated as Eq. (40).

$$M(\theta') = -0.29585\theta' - 0.53762|\theta'|\theta'$$
$$r(\theta) = -3.39896\theta^3 + 53.25\theta^5 \tag{40}$$

Table 7. Coefficients from roll histories with different angle of list (Fr = 0).

$\theta_{\alpha 0}$/deg	T/s	T^*	I_{xx} (kg · m)	I^*_{xx}
2.5	1.6125	7.9361	2.6609	0.1975
5	1.6187	7.9669	2.6815	0.199
7.5	1.625	7.9976	2.7023	0.2005
10	1.6275	8.0099	2.7106	0.2012
12.5	1.6425	8.0837	2.7608	0.2049
15	1.6387	8.0653	2.7482	0.204
20	1.6375	8.0591	2.744	0.2036

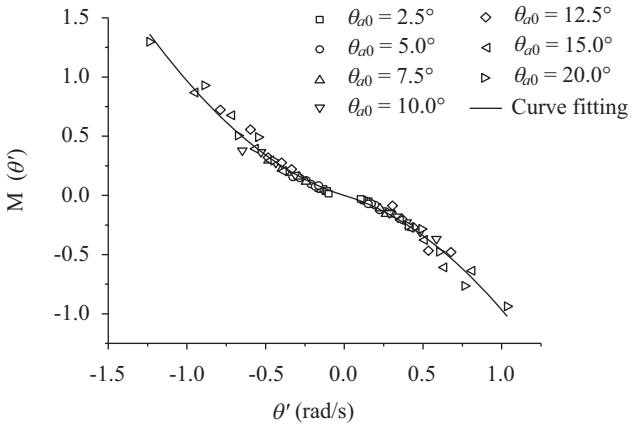

Fig. 8. $M(\theta')$ **for different angle of list with Fr = 0.**

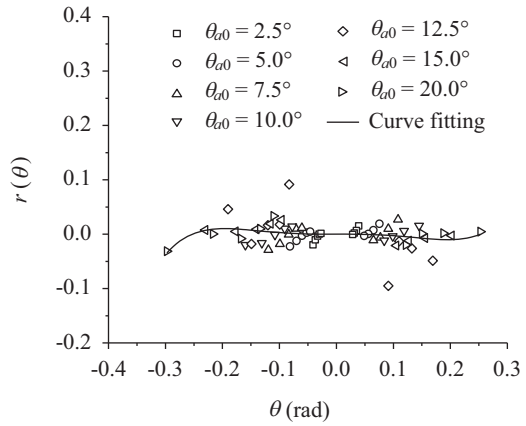

Fig. 9. $r(\theta)$ **for different angle of list with Fr = 0.**

By substituting the form of Eq. (40) into Eq. (8), another new form of the motion equation can be derived as

$$I_{xx}\theta'' + 2N\theta' + D_2\left|\theta'\right|\theta' + C\theta + R_3\theta^3 + R_5\theta^5 = 0 \qquad (41)$$

in which, the value of C is set as 40.4 N/rad (Wilson et al., 2006). Divide Eq. (41) by I_{xx}:

$$\theta'' + 2n\theta' + d_2\left|\theta'\right|\theta' + \omega_0^2\theta + r_3\theta^3 + r_5\theta^5 = 0 \qquad (42)$$

Table 8. Nonlinear damping and restoring (Fr = 0).

$2n$	d_2	r_3	r_5
0.1093	0.1987	1.2563	-19.6817

Table 9. Grid number for different model scale (Fr = 0).

scale	Number of grids (10^4)	
	Background region	Overset region
46.588	24.12	68.61
35.482	22.48	90.96
24.830	24.09	110.63
13.311	23.09	107.57

where

$$2n = \frac{2N}{I_{xx}},\ d_2 = \frac{D_2}{I_{xx}},\ \omega_0^2 = \frac{C}{I_{xx}},\ r_3 = \frac{R_3}{I_{xx}},\ r_5 = \frac{R_5}{I_{xx}} \qquad (43)$$

The roll period and virtual moment of inertia are tabulated in Table 7, where the non-dimensional coefficients of roll period and virtual moment of inertia are defined, respectively, as

$$T^* = T\sqrt{\frac{g}{B}} \quad I_{xx}{}^* = \frac{I_{xx}}{m \cdot B^2} \qquad (44)$$

It's found that the influence of the angle of list on the roll period is negligible from Table 7. This is consistent with the objective fact that the roll period, which depends on the geometry of the ship and the mass distribution, is an intrinsic property of the ship. Little influence of the angle of list on the virtual moment of inertia is also observed. Substitute the average of these values into Eq. (43) to obtain the nonlinear damping and restoring coefficients, as tabulated in Table 8.

3. Influence of Model Scale

The scale effect is always an inevitable problem that exists between the model and the real ship, because their Re numbers are not equal. The influence of the model scale on the free roll decay at Fr = 0 is studied in this section, and the model scale λ ranges from 13 to 47. The details of the grid numbers for different scale models are listed in Table 9.

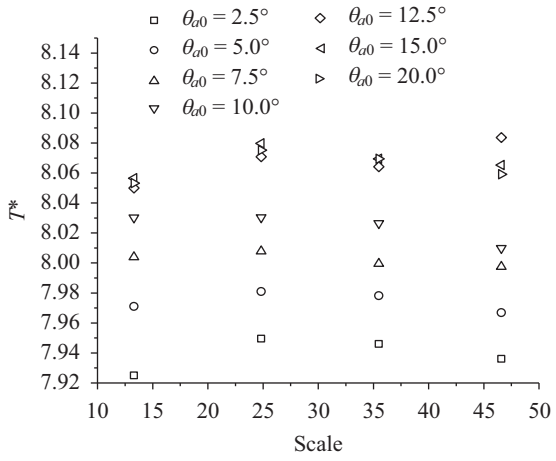

Fig. 10. Time period for λ s (Fr = 0).

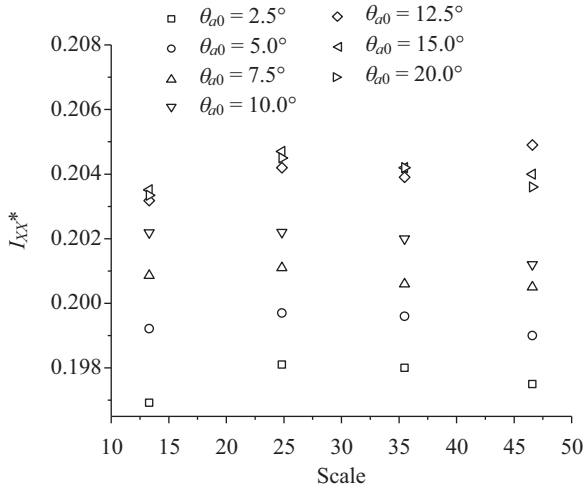

Fig. 11. Virtual moment of inertial for λ s (Fr = 0).

The dimensionless roll period and virtual moment of inertia are showed in Figs. 10 and 11, respectively. Results illustrate that the influence of the model scale on the roll period and the virtual moment inertia coefficients is small. Given that a model scale is fixed, the roll period increases with the angle of list if angle of list is less than 10°, while it almost keeps constant if angle of list ranges from 12.5° to 20°. This rule also holds for the virtual moment of inertia.

By solving the inverse problem, the nonlinear damping and restoring force are derived, as scattered in Figs. 12 and 13, and their corresponding coefficients are listed in Table 10. Roll damping is composed of two components, a linear and a nonlinear one, but the nonlinear term is subdominant. Linear damping is in proportion to $\sqrt{\lambda}$, and nonlinear damping has a reduced tendency as λ decreases.

As to the nonlinear restoring force, it is composed of r_3 and r_5 approximately, the r_5 term is subdominant as the roll angle is less than 1 rad. For the model whose scale is 46.588, its linear restoring force is 40.4 N*m and its related r_3 is small, which

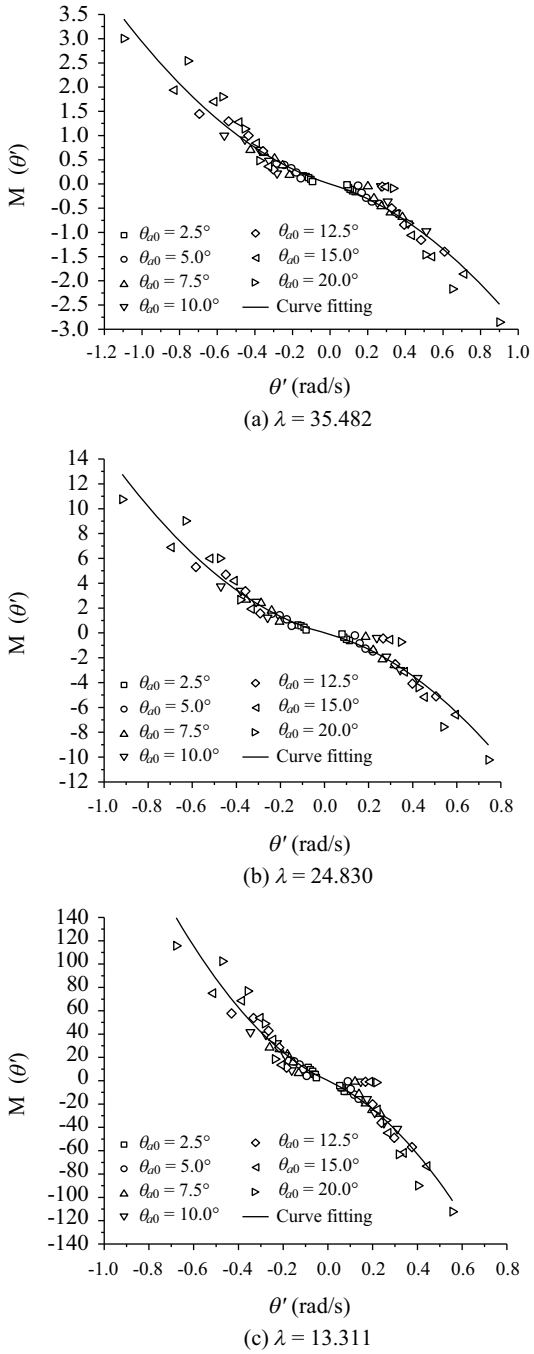

Fig. 12. Nonlinear damping for λ s (Fr = 0).

means that the linear restoring force is proper. However, r_3 increases as the scale decreases, and its growth rate is greater than that of r_5.

In a word, the roll damping decreases slightly with the scale, while the nonlinear restoring force increases as the scale decreases.

2. Influence of Ship Speed

The influences of the angle of list and the model scale were studied in previous two sections at Fr = 0, this section will

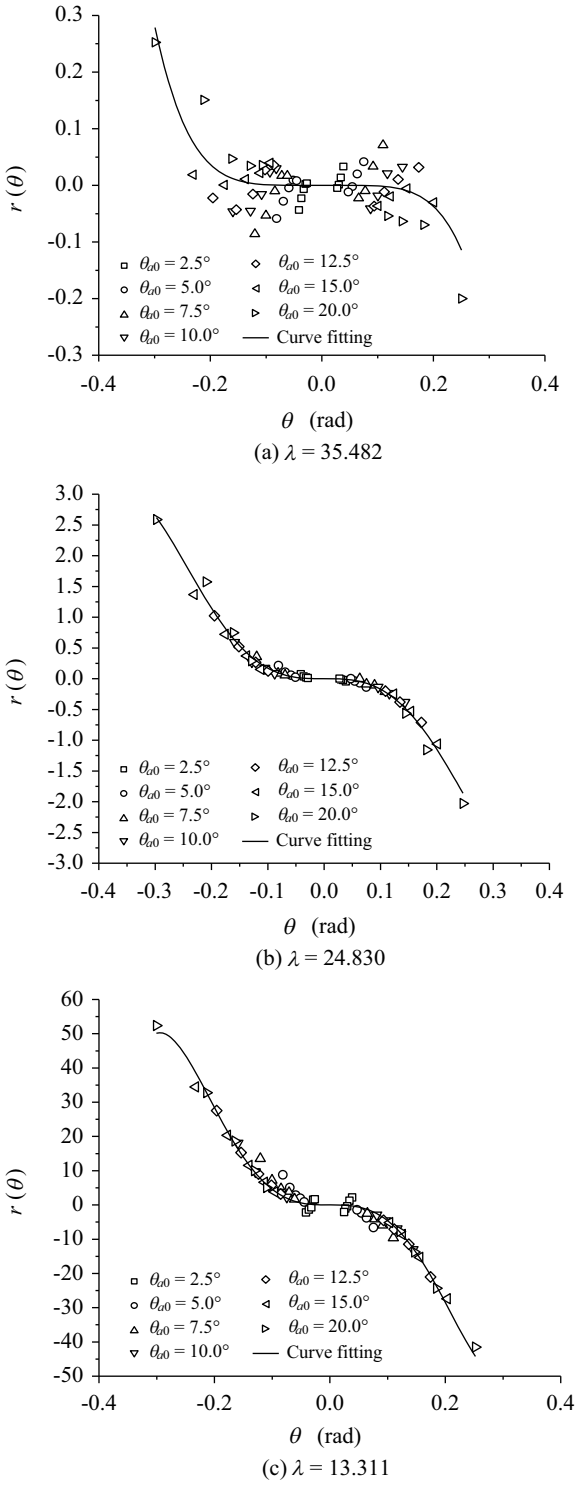

(a) λ = 35.482

(b) λ = 24.830

(c) λ = 13.311

Fig. 13. Non-linear restoring force for λ s (Fr = 0).

focus on the influence of ship speed (Fr = 0.138, 0.28) given that the model scale is 46.588. The grid numbers for the numerical simulations at different speeds are listed in Table 11.

The roll period is obtained from the time history of the roll angle. The virtual moment of inertia is evaluated according to the third equation in Eq. (43). Results are tabulated in Table 12. It's found that the roll period and the virtual moment of inertia decrease slightly as speed increases.

Table 10. Nonlinear damping and restoring coefficients for λ s.

scale	$2n$	d_2	r_3	r_5
46.588	0.1107	0.2467	0.8757	-12.6223
35.482	0.0979	0.2801	2.7021	-20.7265
24.830	0.0721	0.1609	2.8348	-14.3093
13.311	0.0609	0.1234	3.4507	-23.8550

Table 11. Grids numbers for different Fr.

Fr	Number of grids (10^4)	
	Background region	Overset region
0	24.12	68.61
0.138	22.70	73.05
0.28	27.38	69.71

Table 12. Influence of Fr on roll period and virtual inertia moment.

Fr	T/s	T*	I_{xx} (kg · m^2)	I^*_{xx}
0	1.6289	8.0169	2.7155	0.2015
0.138	1.6138	7.9422	2.6650	0.1978
0.28	1.5996	7.8728	2.6187	0.1943

Table 13. Influence of Fr on damping and restoring coefficients.

Fr	$2n$	d_2	r_3	r_5
0	0.1107	0.2467	0.8757	-12.6223
0.138	0.3645	-0.0252	-4.7096	34.8178
0.28	0.5663	-0.0682	-20.9633	218.8236

The nonlinear damping and restoring force are derived by solving the inverse problem, as shown in Figs. 14 and 15, and the corresponding coefficients are listed in Table 13. Roll damping increases slightly with speed, especially the linear component. Ikeda et al. (1978) supposed that the roll damping consists of five damping components, friction damping (Ikeda et al., 1976), wave damping, eddy damping (Ikeda et al., 1977), lift damping and bilge keel damping (Ikeda et al., 1976; Ikeda et al., 1977). Speed mainly affects wave damping and lift damping, these two components are proportional to the angular velocity.

As for the nonlinear restoring force, an interesting phenomenon is detected in Fig. 15. The nonlinear restoring force is in the same direction as the roll angle, which means that a positive/negative roll angle results in a positive/negative nonlinear re-

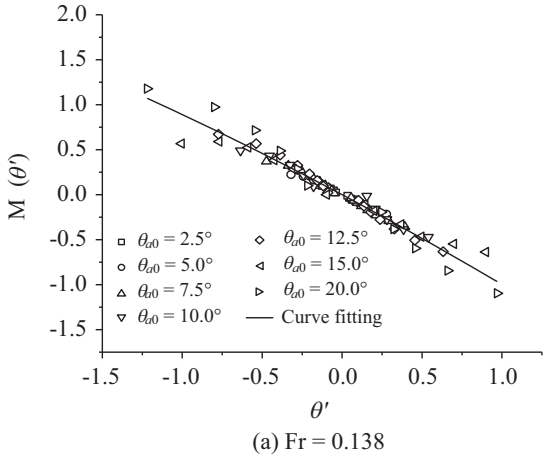

(a) Fr = 0.138

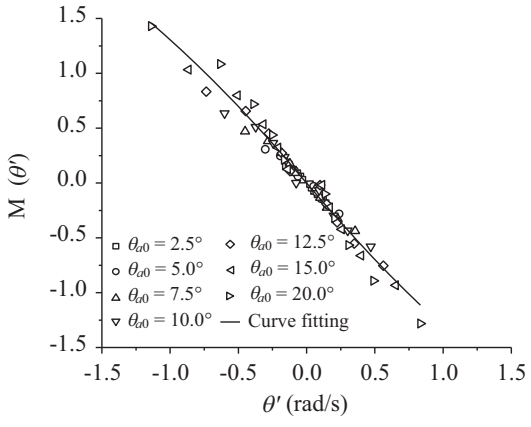

(b) Fr = 0.28

Fig. 14. nonlinear damping.

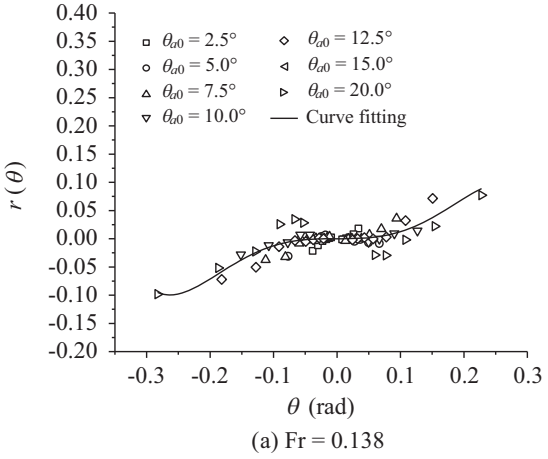

(a) Fr = 0.138

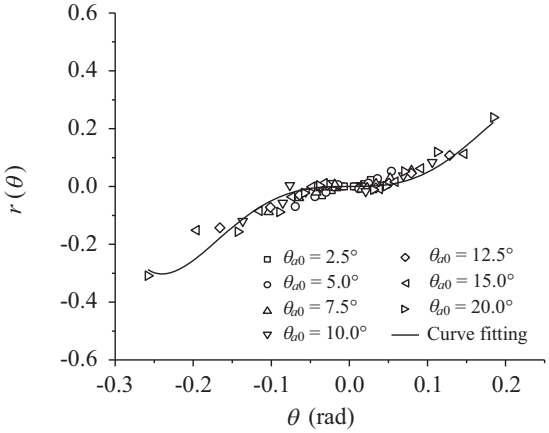

(b) Fr = 0.28

Fig. 15. Nonlinear restoring force.

storing force. This is why there is a larger minus correction from r_3 to the linear restoring force as speed improves, as shown in Table 13. For the hull in navigation, the speed has an influence on the attitude (sinkage and trim) of the hull, then the attitude leads to an area variation of the waterplane, which varies the restoring force. The linear restoring force at Fr = 0 is not suitable to describe the restoring force feature of the hull with speed, because the restoring force decreases as speed increases.

In short, roll damping increases with speed, while the restoring force decreases as the speed increases.

VI. CONCLUSION

Based on Computational Fluid Dynamics combined with the overset technology, the problems of characteristics of the nonlinear damping and restoring forces are investigated. A numerical simulation of the free roll decay is performed for the DTMB 5512 at Fr = 0.138 with an angle of list of $\theta_{\alpha 0} = 10°$ to validate the numerical method in the present paper. The nonlinear damping and restoring force terms are derived by solving a Volterra integral equation of the first kind by using Tikhonov's regularization method. Furthermore, the influences of the angle of list, the model scale, and the ship speed on the roll damping and nonlinear restoring forces are explored. The conclusions, based on CFD numerical simulations, are summarized as:

For the case of the DTMB 5512 at Fr = 0.138 with an angle of list of $\theta_{\alpha 0} = 10°$, the computational roll history shows a good quantitative agreement with the experimental one. The numerical result of the natural roll period is 1.6125 s and the experimental value is 1.6402 s, the error of these is less than 2%. The computation of the free roll decay with overset mesh is feasible. It's an ingenious method to obtain the nonlinear damping and restoring forces by solving the inverse problem from time histories of the roll angle and the roll angular velocity. The result indicates that the regularization parameter $\chi^2 = 0.01$ is proper.

It's found that the influence of the angle of list on the roll period and virtual moment of inertia is negligible. Roll damping decreases with model scale slightly, due to the decrease of its subdominant component, nonlinear damping. However, roll damping increases with speed because its dominant component, linear damping, increases as speed increases.

As for the characteristics of the nonlinear restoring force, it can be concluded that the nonlinear restoring force increases as the model scale decreases, while it decreases as the speed increases.

ACKNOWLEDGEMENTS

This work has been supported by National Natural Science Foundation of China (NSFC, Grant no. 51479117, 51579147) and National Key Basic Research Program of China (973 Program, Grant no. 2014CB046203)

REFERENCES

Aloisio, G. and F. Felice (2006). PIV analysis around the bilge keel of a Ship model in a free roll decay. XIV Congresso Nazionale AI VE. LA., Rome, Italy, Nov.

CD-adapco (2014). User guide STAR-CCM+ version 8.04.

Chen, H. C., T. Liu and E. T. Huang (2001). Time-domain simulation of large amplitude ship roll motions by a chimera RANS method. The Eleventh International Offshore and Polar Engineering Conference, International Society of Offshore and Polar Engineers.

de Oliveira, A. C. and A. C. Fernandes (2014). The nonlinear roll damping of a FPSO hull. Journal of Offshore Mechanics and Arctic Engineering 136(1), 011106.

Groetsch, C. W. (1993). Inverse problems in the mathematical sciences. Vol. 52.: Springer.

Hou, X. and Z. Zou (2015). SVR-based identification of nonlinear roll motion equation for FPSOs in regular waves. Ocean Engineering 109, 531-538.

Hou, X. and Z. Zou (2016). Parameter identification of nonlinear roll motion equation for floating structures in irregular waves. Applied Ocean Research 55, 66-75.

http: //www.simman2008.dk/5415/5415_geometry.htm.

Ikeda, Y., K. Komatsu, Y. Himeno and N. Tanaka (1977). On roll damping force of ship-effect of hull surface pressure created by bilge keels. Journal of Kansai Society of Naval Architects 165, 31-40.

Ikeda, Y., Y. Himeno and N.Tanaka (1976). On roll damping force of ship: effects of friction of hull and normal force of bilge keels. Journal of Kansai Society of Naval Architects 161, 41-49.

Ikeda, Y., Y. Himeno and N. Tanaka (1977). On eddy making component of roll damping force on naked hull. Journal of Japan Society of Naval Architects 162, 59-69.

Ikeda, Y., Y. Himeno and N. Tanaka (1978). A prediction method for ship roll damping. Report of the Department of Naval Architecture, University of Osaka Prefecture (00405).

Irvine Jr, M. (2004). Towing tank tests for surface combatant for coupled pitch and heave and free roll decay motions.

Irvine, M., J. Longo and F. Stern (2013). Forward speed calm water roll decay for surface combatant 5415: global and local flow measurements. Journal of Ship Research 57(4), 202-219.

Jang, T. S. (2011). Non-parametric simultaneous identification of both the nonlinear damping and restoring characteristics of nonlinear systems whose dampings depend on velocity alone. Mechanical Systems and Signal Processing 25(4), 1159-1173.

Jang, T. S. (2013). A method for simultaneous identification of the full nonlinear damping and the phase shift and amplitude of the external harmonic excitation in a forced nonlinear oscillator. Computers & Structures 120, 77-85.

Jang, T. S., H. S. Choi and S. L. Han (2009). A new method for detecting non-linear damping and restoring forces in non-linear oscillation systems from transient data. International Journal of Non-Linear Mechanics. 44(7), 801-808.

Jang, T. S., S. H. Kwon and J. H. Lee (2010). Recovering the functional form of the nonlinear roll damping of ships from a free-roll decay experiment: an inverse formulism. Ocean Engineering 37(14), 1337-1344.

Jiang, Y., R. C. Zhu, G. P. Miao and C. L. Yang (2016). Damping prediction of a rolling ship with bilge keel in viscous flow based on numerical simulation. Ship Building of China 57(2), 1-12.

Jiang, Y., R. C. Zhu, G. P. Miao, J. Fan and C. Ma (2016). Study on ship roll damping. The Second Conference of Global Chinese Scholars on Hydrodynamics. Wuxi.

Li, J. L., S. L. Yang and S. Pang (2012). Free roll decay modeling of a trimaran based on least square support vector machine. Oceans, 2012, IEEE.

Ma, S, Y. Cao, W. X. Ma, W. Y. Duan and R. F. Wang (2012). Investigation of estimation method for roll damping from calm water free decay experiment using energy method. Journal of Ship Mechanics 16(10), 1122-1130.

Stern, F., R. V. Wilson, H. W. Coleman and E. G. Paterson (1999). Verification and validation of CFD simulations. Iowa Institute of Hydraulic Research, The University of Iowa, IIHR Report (407).

Stern, F., R. V. Wilson, H. W. Coleman and E. G. Paterson (2001). Comprehensive approach to verification and validation of CFD simulations-part 1: methodology and procedures. Journal of fluids engineering 123(4), 793-802.

Taylan, M. (2000). The effect of nonlinear damping and restoring in ship rolling. Ocean Engineering. 27(9), 921-932.

Tikhonov (1963). A. Solution of incorrectly formulated problems and the regularization method. in Soviet Math. Doklady 4. 1035-1038.

Wilson, R. V., F. Stern, H. W. Coleman and E. G. Paterson (2001). Comprehensive approach to verification and validation of CFD simulations-Part 2: Application for RANS simulation of a cargo/container ship. Journal of fluids engineering 123(4), 803-810.

Wilson, R. V., P. M. Carrica and F. Stern (2006). Unsteady RANS method for ship motions with application to roll for a surface combatant. Computers & fluids 35(5), 501-524.

Yang, C. L., R. C. Zhu, G. P. Miao and J. Fan (2012). A roll damping prediction method of three-dimensional ships based on CFD computation. Journal of Shanghai Jiaotong University 8, 003.

Yang, C. L., R. C. Zhu, G. P. Miao and J. Fan (2013). Numerical simulation of rolling for 3-D ship with forward speed and nonlinear damping analysis. Journal of Hydrodynamics, Ser. B 25(1), 148-155.

Zhou, L. S. (2012). Theoretical and experimental research on roll damping of the displacement type vessel. Harbin, Harbin Engineering University.

Zhu, R. C., C. L. Yang, G. P. Miao, H. P. Fu and L. B. Lv (2012). Numerical simulation of 3-D ship body rolling and damping calculation in viscous flow. Proceedings of the 11st National Congress on Hydrodynamics & 24th National Conference on Hydrodynamics and commemoration of the 110th aniversary of Zhou Pei-yuan's birth.

Zhu, R. C., C. L. Yang, G. P. Miao and J. Fan (2015). Computational fluid dynamics uncertainty analysis for simulations of roll motions for a 3D ship. Journal of Shanghai Jiaotong University (Science) 20, 591-599.